Chapter 6

Electrical and photovoltaic properties of $La_{1-x}Sr_xMnO_3$/Nb:$SrTiO_3$ junctions

6.1 Introduction

Heterostructures of transition metal oxides have attracted much interest in the research of oxide electronics, which aim at utilizing the unique electrical properties at heterointerfaces such as the electrically induced reversible resistance switching in $SrRuO_3$/Nb : $SrTiO_3$ [49] or the large magnetocapacitance in $La_{0.7}Sr_{0.3}MnO_{3-\delta}$/Nb:$SrTiO_3$ [50]. These phenomena indicate that the electrical properties of oxide heterostructures are strongly affected by those of the bulk oxides. In this chapter, from the viewpoint of photocarrier injection, we study the electrical and photovoltaic properties of $La_{1-x}Sr_xMnO_3$/Nb : $SrTiO_3$ junctions as examples of oxide heterojunctions. By comparison with the case of Au/Nb : $SrTiO_3$ or by varying x in $La_{1-x}Sr_xMnO_3$, we aim at revealing the effect of the physical properties of oxides on the electrical and photovoltaic properties at the interface.

6.2 Physical properties of $La_{1-x}Sr_xMnO_3$

6.2.1 Transport properties

Transport properties of the perovskite manganites are explained by the complex mixing of various parameters, such as lattice distortion and magnetism. Among them, one important concept is the double-exchange (DE) interaction. The perovskite manganites have the general formula $RE_{1-x}AE_xMnO_3$ where RE is usually a trivalent rare earth ion and AE is a divalent alkaline rare earth ion. Octahedral coordination by oxygen ions induces the splitting of the $3d$ orbitals of Mn to t_{2g} orbital states and e_g orbital states. Lattice distortions driven by the Jahn-Teller effect induce further splitting of t_{2g} and e_g levels (Fig. 6.1 (a)) in the case of $t_{2g}^3 e_g^1$ configuration. In the case of $x = 0$, three electrons are filled in the t_{2g} states and one electron is filled in the e_g states of each Mn ion. Because

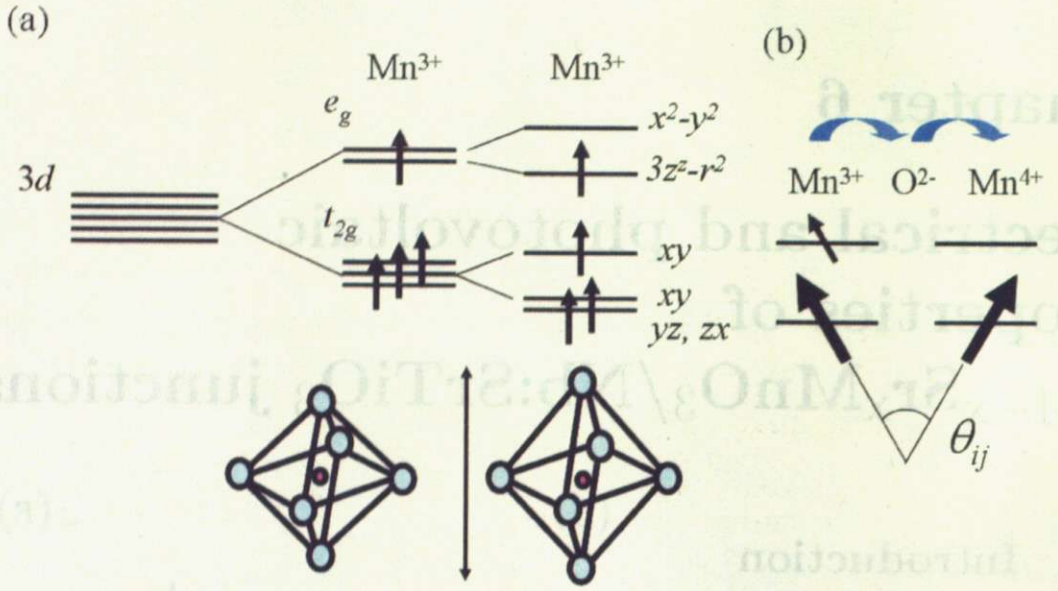

Figure 6.1: (a) Splitting of $3d$ orbitals caused by the octahedral coordination of O^{2-}. In the case of Mn^{3+}, three electrons are filled in the t_{2g} levels and one electron is filled in the e_g level. The e_g and t_{2g} levels are further splitted by Jahn-Teller distortion. (b) Schematic image of the DE interaction. Effective hopping interaction is determined by the relative angles of the spins of the localized electrons in the t_{2g} levels.

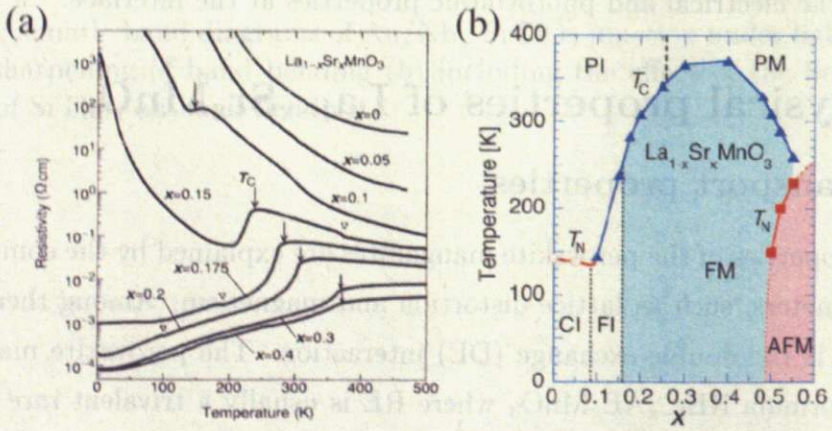

Figure 6.2: (a) Temperature dependent resistivity of $La_{1-x}Sr_xMnO_3$ single crystals [51]. (b) Magnetic phase diagram of the $La_{1-x}Sr_xMnO_3$ system [52].

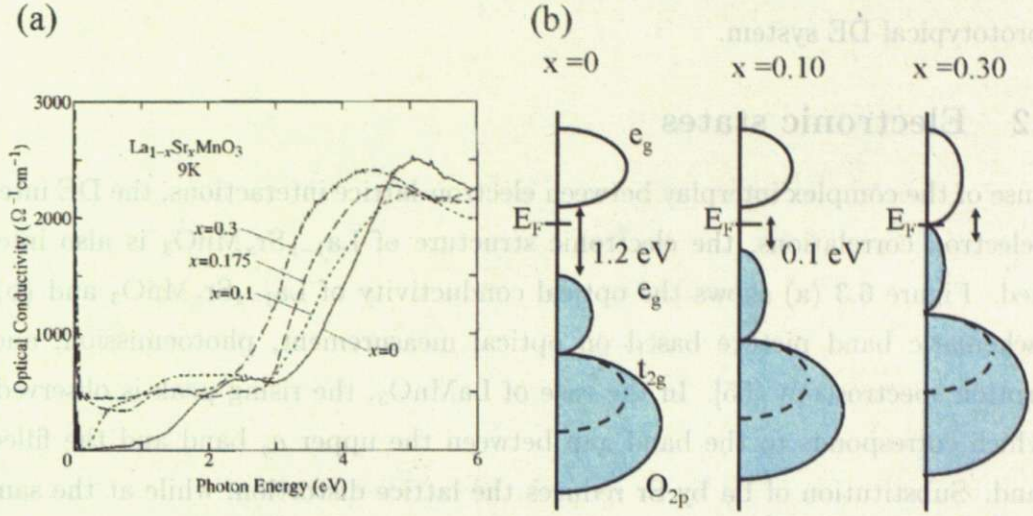

Figure 6.3: (a) Optical conductivity of $La_{1-x}Sr_xMnO_3$ ($0 \leq x \leq 0.30$) measured at 9 K [54] and (b) schematic band structure of $La_{1-x}Sr_xMnO_3$. The band gap of $LaMnO_3$ is 1.2 eV and substitution of La by Sr reduces the gap. At $x = 0.10$, the band gap is reduced to 0.1 eV and the gap disappears at $x \geq 0.175$.

of the electron correlation effect, electrons in e_g states are localized.

Spins in the $3d$ orbitals are strongly coupled between the t_{2g} localized electron spin ($S = 3/2$) and the conduction electron spin ($S = 1/2$) by Hund's coupling. This Hund's coupling energy is as large as 2-3 eV in manganites and this is larger than the inter-site hopping interaction of electrons in e_g states, t_{ij}^0. Under this condition, the effective hopping interaction is described as

$$t_{ij} = t_{ij}^0 \cos\left(\frac{\theta_{ij}}{2}\right) \tag{6.1}$$

where θ_{ij} is the relative angle of the neighboring spins. Schematic image of hopping by DE interacton is shown in Fig. 6.1 (b). This relation implies the ferromagnetic order via conduction electrons.

Figure 6.2 shows the temperature dependence of the resistivity in $La_{1-x}Sr_xMnO_3$ system and its magnetic phase diagram. The parent material, $LaMnO_3$, is an antiferromagnetic insulator below 120 K. e_g states on the Mn sites are filled by one electron and are localized by the onsite Coulomb repulsion and the Jahn-Teller distortion. Hole doping by substitution of La for Sr induces $La_{1-x}Sr_xMnO_3$ to become a ferromagnetic metal around $x = 0.17$, associated with an insulator to metal transition mediated by the DE interaction. The Curie temperature becomes as high as 370 K around $x = 0.30$. The transport properties of perovskite manganites is also strongly affected by the lattice distortion, especially in, for example, $Pr_{1-x}Ca_xMnO_3$ and $La_{1-x}Ca_xMnO_3$ [53]. However, the effect of

lattice distortion is smallest in $La_{1-x}Sr_xMnO_3$ system, so this system can be thought as the prototypical DE system.

6.2.2 Electronic states

Because of the complex interplay between electron-lattice interactions, the DE interaction and electron correlations, the electronic structure of $La_{1-x}Sr_xMnO_3$ is also intensively studied. Figure 6.3 (a) shows the optical conductivity of $La_{1-x}Sr_xMnO_3$ and (b) shows the schematic band picture based on optical measurement, photoemission, and x-ray absorption spectroscopy [55]. In the case of $LaMnO_3$, the rising peak is observed at 1.2 eV which corresponds to the band gap between the upper e_g band and the filled lower e_g band. Substitution of La by Sr reduces the lattice distortion, while at the same time doping holes to the e_g band, this reducing the gap between 2 e_g states. The gap is reduced to 0.1 eV in $x = 0.10$ and disappear at $x \geq 0.175$.

6.3 Experimental

We measured the electrical properties and photovoltaic properties of different composition of $La_{1-x}Sr_xMnO_3/Nb : SrTiO_3$ (0.01 wt %) junctions ($x = 0.10, 0.15, 0.20$, and 0.30). 600 Å $La_{1-x}Sr_xMnO_3$ films were grown by pulsed laser deposition (PLD) at the O_2 partial pressure of 1 mTorr and a substrate temperature of 750 °C. using a KrF excimer laser (Lambda Physik AG COMPex 201) as the ablation laser. Pulse frequency was 4 Hz and the laser energy at the target surface was $\sim$ 30 mJ. Ag wires were placed on the $La_{1-x}Sr_xMnO_3$ films with Ag paste and Al wire was ultra-sonic soldered to the $Nb : SrTiO_3$ as ohmic electrodes. Typical dimensions of the junctions were 1 mm^2.

6.4 Results and discussion

Electrical properties

Figure 6.4 shows the temperature dependent I-V characteristics of different composition $La_{1-x}Sr_xMnO_3/Nb : SrTiO_3$ junctions. Rectifying behavior is observed at all junctions. Because of the insulating property of $La_{0.9}Sr_{0.1}MnO_3$, the I-V characteristics of $La_{0.9}Sr_{0.1}MnO_3/Nb : SrTiO_3$ are strongly affected by the series resistance as seen in the strong temperature dependence in its I-V characteristics at large forward voltage. Unlike $Au/Nb : SrTiO_3$ junctions, none of these junctions exhibited anomalous feature of the I-V characteristics at low temperature. The temperature dependence of the tunneling contribution E_0, which is calculated by $E_0 = q/(\partial \ln J/\partial V)$ from the I-V curves are shown in Fig. 6.5. Except for $La_{0.9}Sr_{0.1}MnO_3$, the temperature dependent E_0 is well

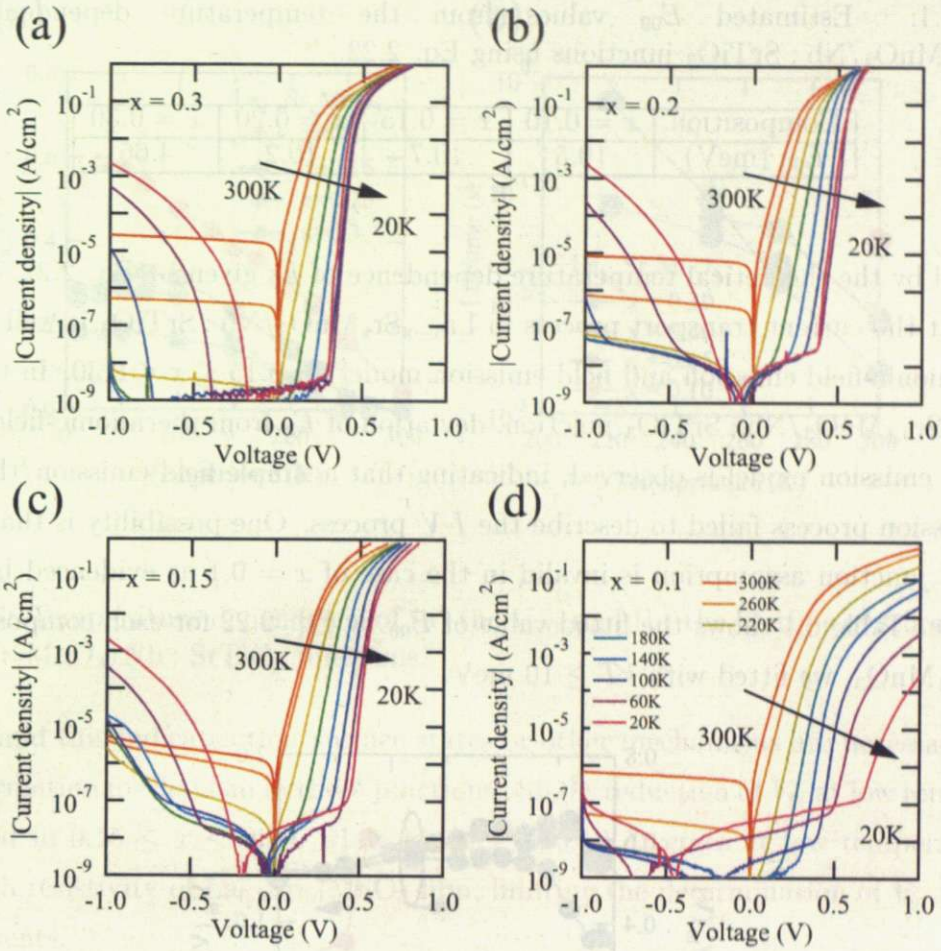

Figure 6.4: Temperature dependent I-V characteristics of $La_{1-x}Sr_xMnO_3/Nb : SrTiO_3$ junctions (a) $x = 0.3$, (b) $x = 0.2$ (c) $x = 0.15$ (d) $x = 0.10$. The I-V characteristics were measured every 40 K from 300 K to 20 K.

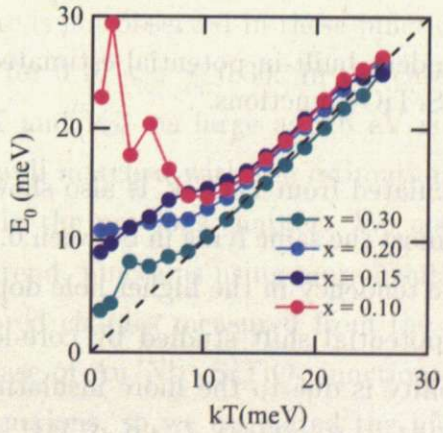

Figure 6.5: Temperature dependent tunneling contribution E_0 estimated from the I-V characteristics of $La_{1-x}Sr_xMnO_3/Nb : SrTiO_3$ junctions using $E_0 = 1/q(\partial \ln J/\partial V)$.

Table 6.1: Estimated E_{00} values from the temperature dependent E_0 of $La_{1-x}Sr_xMnO_3/Nb : SrTiO_3$ junctions using Eq. 2.22.

Composition	$x = 0.10$	$x = 0.15$	$x = 0.20$	$x = 0.30$
E_{00} (meV)	10.5	10.7	10.2	4.66

explained by the theoretical temperature dependence of E_0 given by Eq. 2.22. This indicates that the current transport process in $La_{1-x}Sr_xMnO_3/Nb : SrTiO_3$ is well expressed by thermionic-field emission and field emission model for $0.15 \leq x \leq 0.30$. In the case of the $La_{0.9}Sr_{0.1}MnO_3/Nb : SrTiO_3$ junction, deviation of E_0 from thermionic-field emission and field emission model is observed, indicating that a simple field emission/thermionic-field emission process failed to describe the I-V process. One possibility is that a simple Schottky junction assumption is invalid in the case of $x = 0.1$ as evidenced by its high resistance. Table 6.1 shows the fitted value of E_{00} by Eq. 2.22 for each composition. For $La_{0.9}Sr_{0.1}MnO_3$, we fitted with $kT \geq 10$ meV.

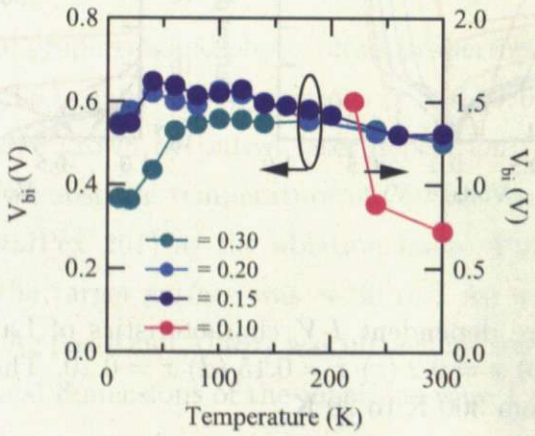

Figure 6.6: Temperature dependent built-in potential estimated from the C-V measurements in $La_{1-x}Sr_xMnO_3/Nb : SrTiO_3$ junctions.

Built-in potential (V_{bi}) calculated from $1/C^2$-V is also shown in Fig. 6.6. V_{bi} in the range of $0.15 \leq x \leq 0.30$ are almost the same lying in between 0.50 V and 0.60 V at 300 K. This result is different from the tendency in the higher hole doping compositions ($0.30 \leq x \leq 1$) [56] or the chemical potential shift studied by core-level X-ray photoemission spectroscopy [57]. One possibility is due to the more insulating behavior at lower hole concentration. Work function of $La_{0.8}Sr_{0.2}MnO_3$ is 4.9 eV [58] and the electron affinity of $SrTiO_3$ is 3.9 eV [29], giving a Schottky barrier height from the Schottky-Mott relation of 1 eV. Since the energy difference between the Fermi level and the conduction band minimum in $Nb:SrTiO_3$ is 6 meV, the measured built in potential is much smaller than

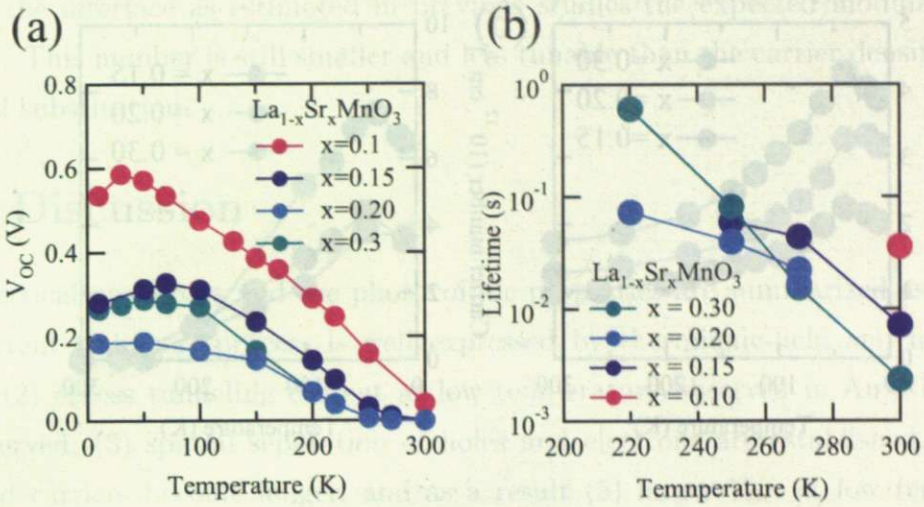

Figure 6.7: Temperature dependence of (a) the V_{OC} and (b) the lifetime of stored charges in $La_{1-x}Sr_xMnO_3/Nb : SrTiO_3$ junctions.

expected and this indicates that surface states or other mechanisms are necessary for the barrier formation mechanism in these junctions. Slight reduction of V_{bi} at low temperature is observed in $0.15 \leq x \leq 0.30$, while V_{bi} in $x = 0.10$ diverges at low temperature due to the high resistivity of $La_{0.9}Sr_{0.1}MnO_3$ film, limiting the determination of V_{bi} from C-V measurements.

Photovoltaic properties

Figure 6.7 (a) shows V_{OC} as a function of temperature in $La_{1-x}Sr_xMnO_3/Nb : SrTiO_3$ junctions. V_{OC} at room temperature is small, but gradually increases with decrease in temperature, similar to the case of $Au/Nb : SrTiO_3$ junctions. However, a rigid decrease of V_{OC} at low temperature is not observed in these junctions, although a slight reduction is observed below 100 K for $0.10 \leq x \leq 0.30$. In the case of V_{OC} in $x = 0.10$, V_{OC} keep increasing down to 30 K and V_{OC} as large as 0.6 eV is observed. These temperature dependences of V_{OC} are well matched with the estimation based on thermionic-field and field emission theory as in the previous chapter. We also observe the composition dependence. As a general trend, junctions using more insulating compounds exhibit larger V_{OC}. The lifetime of stored charges measured from the decay of V_{OC} is also shown in Fig. 6.7 (b). As in the case of $Au/Nb : SrTiO_3$ junctions, we did not observe the linear decay of V_{OC} in these junctions, so we estimated the lifetime from exponential fitting. The maximum lifetime we can measure was in this case about the order of a few seconds. With decreasing the temperature, the lifetime of carriers increases. While the lifetime of stored carriers in $Au/Nb : SrTiO_3$ was dramatically reduced at low temperatures, the

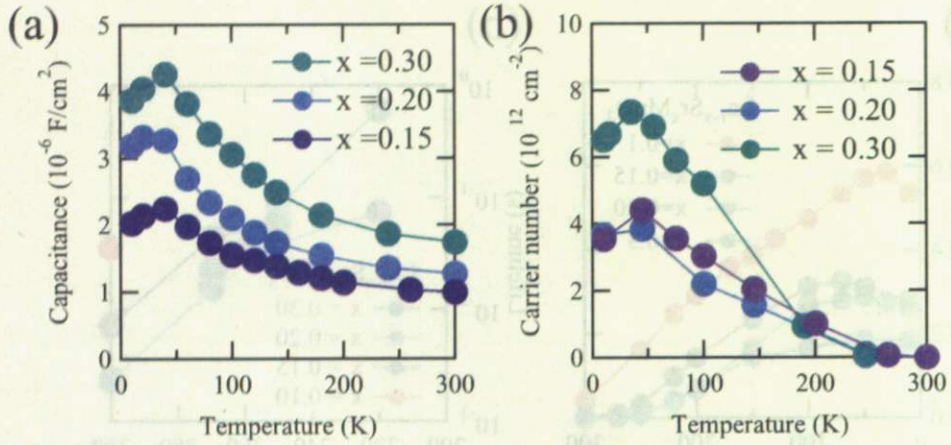

Figure 6.8: (a) Temperature dependent depletion layer capacitance of $La_{1-x}Sr_xMnO_3/Nb:SrTiO_3$ junctions. (b) The number of injected holes estimated from V_{OC} and the depletion layer capacitance.

lifetime of stored charges in $La_{1-x}Sr_xMnO_3/Nb:SrTiO_3$ junctions are more than a few second even at low temperatures.

Figure 6.8 (a) shows the depletion layer capacitance as a function of the temperature and (b) shows the number of holes injected to $La_{1-x}Sr_xMnO_3$ estimated from V_{OC} and the depletion layer capacitance. The depletion layer capacitances gradually increase with decreasing temperature, but turn to decrease at about 50 K. The capacitances at low temperature are only twice as large as those at 300 K despite the permittivity of $SrTiO_3$become about 100 times larger than that of 300 K at zero bias. These results are because of the field dependent permittivity of $SrTiO_3$. One interesting thing is that the depletion layer capacitance of $x = 0.30$ is largest in the range $0.15 \leq x \leq 0.30$, this tendency is opposite to V_{OC}. Although the built-in potential is almost the same, the capacitance is dependent on the composition of $La_{1-x}Sr_xMnO_3$. This may be related to the physical properties of $La_{1-x}Sr_xMnO_3$. One possibility is the existence of the depletion layer in $La_{1-x}Sr_xMnO_3$. Between $0.30 \geq x \geq 0.17$, $La_{1-x}Sr_xMnO_3$ is metallic, so we do not need to consider the depletion layer in the metal according to the model of the Schottky barrier contact. However, if we assume "the depletion layer" in $La_{1-x}Sr_xMnO_3$, in more insulating compounds, the effective mobile carriers can be considered to small, so "the depletion layer" can become larger. This is consistent to the result of capacitance measurements. The number of injected holes is then largest in $x = 0.30$ at low temperatures and exceeds more than $6 \times 10^{12}/cm^2$. If the injected carriers are distributed uniformly in the $La_{1-x}Sr_xMnO_3$ films, the modulated doping level is the order of 10^{17} cm^{-3} and this corresponds to 0.001 % substitution of La by Sr. If the holes are localized in just a few

Å from the interface as estimated in previous studies the expected modulation level is ~ 0.1 %. This number is still smaller and less tunable than the carrier density control by chemical substitution.

6.5 Discussion

The electrical properties and the photovoltaic properties are summarized as follows. (1) The current transport process is well expressed by thermionic-field and field emission theory, (2) excess tunneling current at low temperature observed in $Au/Nb : SrTiO_3$ is not observed, (3) spatial separation of holes and electrons are established, (4) lifetime of stored carriers become longer, and as a result (5) larger V_{OC} at low temperature is observed. The composition dependence of photovoltaic properties are also observed. As a general trend, large V_{OC} is observed in the junction using more insulating $La_{1-x}Sr_xMnO_3$.

First we discuss why excess current is reduced at low temperature in $La_{1-x}Sr_xMnO_3$ $/Nb : SrTiO_3$ junctions, different from $Au/Nb : SrTiO_3$ junctions. The most likely possibility is the difference of the built-in potential. In the case of $Au/Nb : SrTiO_3$ studied in the previous chapter, the built-in potential is 1.2 eV and slightly increased with decreasing the temperature. On the other hand, except for $x = 0.10$, V_{bi} of $La_{1-x}Sr_xMnO_3$ were about 0.6 eV at 300 K and decreases to 0.4 eV below about 50 K. Sharpening of the band bending is more significant for larger built-in potential because of the larger electric field at the interface.

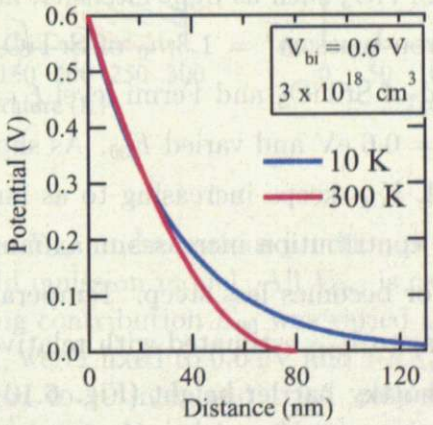

Figure 6.9: Simulation of temperature dependent potential barrier at the interface of $La_{1-x}Sr_xMnO_3$ and $Nb : SrTiO_3$. V_{bi} and doping concentration of $SrTiO_3$ is fixed to 0.6 V and 3×10^{18} cm^3.

Figure 6.9 shows the calculated potential variation from $La_{1-x}Sr_xMnO_3/Nb$:$SrTiO_3$ interface using Eq. 3.4 in which the electric field dependence and the temperature depen-

dence of the permittivity of $SrTiO_3$ is taken into consideration. We fixed V_{bi} and doping concentration of $SrTiO_3$ to 0.6 V and 3×10^{18} cm^3. As shown in the figure, the barrier shape at 300 K and 10 K is almost the same and sharpening of the band bending is not observed. The permittivity of the $SrTiO_3$ is strongly affected by the electric field and temperature, so the shape of the barrier can be strongly changed, but the band shape is not so changed in $La_{1-x}Sr_xMnO_3/Nb : SrTiO_3$, so excess current transport is not observed.

Next we discuses the photovoltaic properties with the thermionic-field emission and the field emission model. As already mentioned, band structure of $La_{1-x}Sr_xMnO_3$ is affected by the composition, especially between the metallic compound and insulating compound. In this study, $0.15 \leq x \leq 0.30$ shows almost same electrical and photovoltaic properties and $x = 0.10$ is slightly different from others. So we discuss these two regimes separately.

$0.15 \leq x \leq 0.30$

Figure 6.10 shows the simulation of expected V_{OC} observed in various conditions. We assume that (1) the Schottky barrier is formed at the interface and (2) current transport is expressed by Eq. 2.21 and Eq. 2.22, where J_0 is described as Eq. 2.26 for thermionic-field emission and as Eq. 2.25 for field emission. In this estimation thermionic emission is ignored because we focus on low temperature behavior. (3) Open circuit voltage is roughly estimated with Eq. 5.1. We choose the Schottky barrier height, 0 K tunneling contribution E_{00} and photocurrent density J_L as parameters. The Schottky barrier height and E_{00} represent the junction electrical properties and J_L represents the measurement conditions and physical properties of the $SrTiO_3$ such as light intensity, and carrier generation rate. We assumed an effective electron mass $m^* = 1.3m_0$ of $SrTiO_3$ and energy between the bottom of the conduction band of $SrTiO_3$ and Fermi level $\xi = -6$ meV throughout the simulations. First we fixed $V_{bi} = 0.6$ eV and varied E_{00}. As shown in Fig. 6.10 (a), if the tunneling contribution is small, V_{OC} keeps increasing to as large as V_{bi} with decreasing temperature. As the tunneling contribution increases, maximum V_{OC} is reduced and the temperature dependent behavior becomes less steep. Temperature depence of measured V_{OC} ($0.15 \leq x \leq 0.30$) is similar to V_{OC} estimated with relatively large tunneling contribution. Next we varied the Schottky barrier height (Fig. 6.10 (b)). The maximum V_{OC} changes with the change of the Schottky barrier height, but the temperature dependent behavior is not changed. Figure 6.10 (c) and (d) show the effect of photocurrent on the temperature dependence of V_{OC} under different tunneling contribution. The effect of the photocurrent is more significant at higher temperature when the tunneling contribution is small. In contrast,if the tunneling contribution is relatively large, V_{OC} become larger with increase the photocurrent, but effect on V_{OC} is smaller compared with other parameters.

Compared to these simulations, the temperature dependence of V_{OC} seems to be most

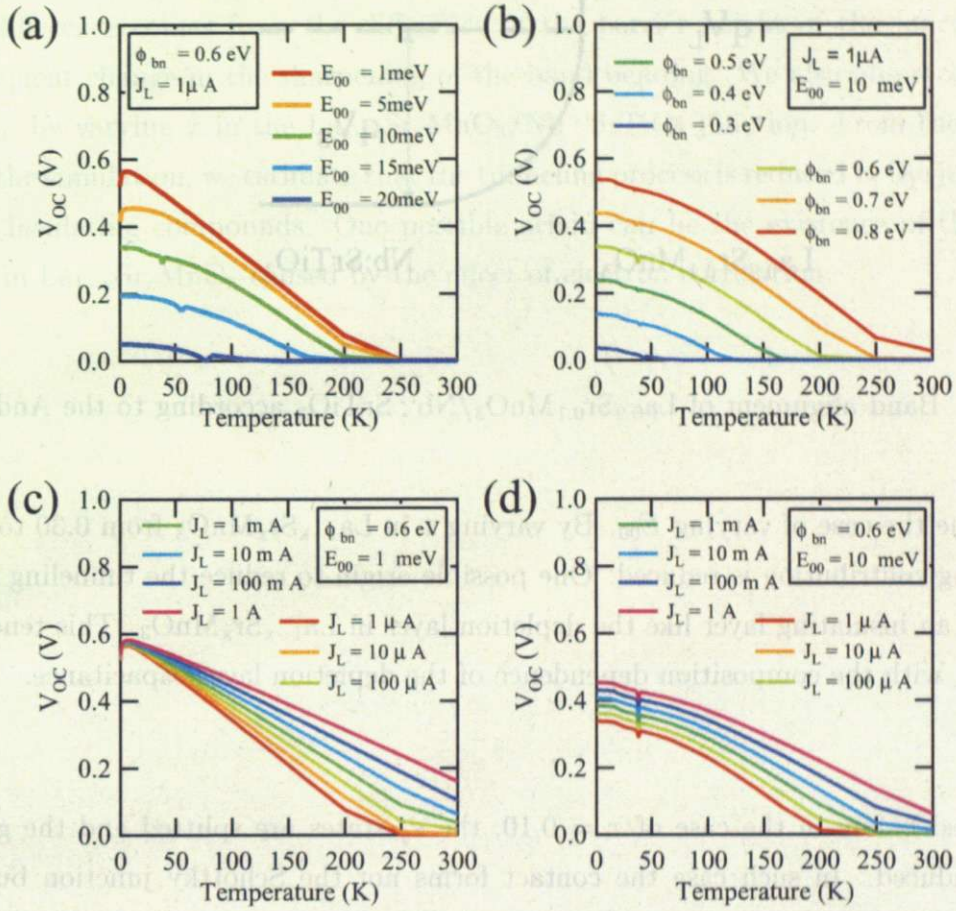

Figure 6.10: The simulated V_{OC} under various junction properties with the assumption of a thermionic-field and field emission model. All V_{OC} is calculated with $m^* = 1.3\,m_0$ and $\xi = -6$ meV. (a) Tunneling contribution E_{00} was varied and the Schottky barrier height, ϕ_{bn}, and photocurrent, J_L, werer fixed to 0.6 eV and 1 μA, respectively. (b)ϕ_{bn} was varied with E_{00} and J_L were fixed to 10 meV and 1 μA, respectively. In (c) and (d), J_L was varied with ϕ_{bn} and E_{00} were 0.6 eV and 1 meV (c), and ϕ_{bn} and E_{00} were 0.6 eV and 10 meV (d). Kinks observed at low temperature are due to discontinuity of the saturation current estimated from thermionic-field emission model and field emission model.

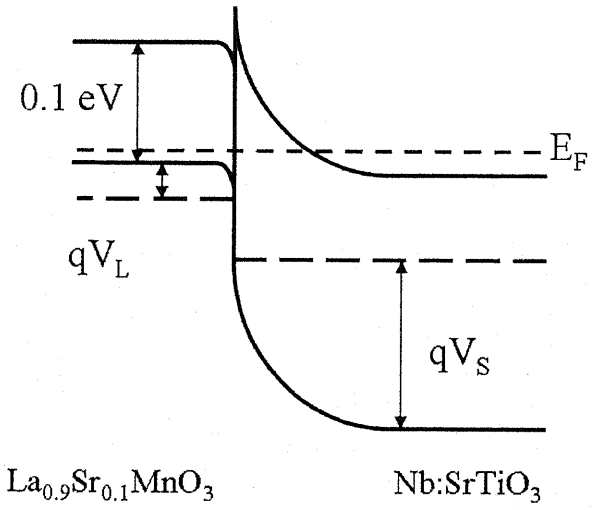

Figure 6.11: Band alignment of $La_{0.9}Sr_{0.1}MnO_3/Nb : SrTiO_3$ according to the Anderson model [59].

similar to the the case of varying E_{00}. By varying x in $La_{1-x}Sr_xMnO_3$ from 0.30 to 0.15, the tunneling contribution is reduced. One possible origin to reduce the tunneling is the existence of an insulating layer like the depletion layer in $La_{1-x}Sr_xMnO_3$. This tendency is consistent with the composition dependence of the depletion layer capacitance.

$x = 0.10$

As mentioned before in the case of $x = 0.10$, the e_g states are splitted and the gap of 0.1 eV is induced. In such case the contact forms not the Schottky junction but the heterojunction. Figure 6.11 shows the band alignment of $La_{0.9}Sr_{0.1}MnO_3/Nb : SrTiO_3$ junction according to Anderson [59]. In the case of the heterojunction we need to consider the built-in potential(V_{bi}) and the depletion layer of both $La_{0.9}Sr_{0.1}MnO_3$ (V_L, W_L) and $SrTiO_3$ (V_S, W_S) respectively. Now we assume that effective carrier density can be much smaller than the doping concentration because carriers are localized by the DE interaction. The depletion layer in $La_{0.9}Sr_{0.1}MnO_3$ is expressed by

$$W_L = \sqrt{\frac{2N_S\epsilon_S\epsilon_L(V_{bi} - V)}{qN_L(\epsilon_S N_S + \epsilon_L N_L)}}$$

where N_S, N_L, ϵ_S, ϵ_L and V are the carrier density of $Nb : SrTiO_3$ and $La_{0.9}Sr_{0.1}MnO_3$, the permittivity of $Nb : SrTiO_3$, $La_{0.9}Sr_{0.1}MnO_3$ and applied voltage to the junction. This depletion layer reduces the tunneling probability, and as a result, larger V_{OC} may be observed.

6.6 Conclusion

In this chapter we have studied the electrical and photovoltaic properties of $La_{1-x}Sr_xMnO_3$ /Nb : $SrTiO_3$ junctions to reveal the effect of correlated oxides in comparison with sample metals. By comparing with Au/$SrTiO_3$, we observed the significant enhancement of V_{OC} at low temperatures in $La_{1-x}Sr_xMnO_3$/Nb : $SrTiO_3$ junctions. The main origin of this difference comes from the difference of the barrier height of the junction and the consequent change in the sharpening of the band bending. We also observed the change of V_{OC} by varying x in the $La_{1-x}Sr_xMnO_3$/Nb : $SrTiO_3$ junction. From the comparison with the simulation, we estimate that the tunneling process is reduced in the junction using more insulating compounds. One possible origin can be the existence of the insulating layer in $La_{1-x}Sr_xMnO_3$ caused by the effect of electron correlation.

Chapter 7

Conclusion

In this study, in order to obtain detailed understanding of the photocarrier injection method as a technique of carrier density modulation in transition metal oxides, we studied electrical properties of several junctions using $SrTiO_3$ from various aspects.

First we studied the electrical properties of $Au/SrTiO_3$ junctions under light irradiation. By irradiating light to the interface from the $SrTiO_3$ side, we confirmed rectifying behavior as in a Schottky junction, suggestive of band bending by photocarrier doping in insulating $SrTiO_3$. There are several reports of photocarrier injection using insulating $SrTiO_3$ substrates, so this result can be useful for understanding the detailed process of photocarrier injection in such structures. Secondly, in order to reveal the effect of temperature and the electric field dependent dielectric permittivity in $SrTiO_3$ on the photovoltaic properties, we studied the photovoltaic properties of $Au/Nb : SrTiO_3$ junctions in relation with their electrical properties. At low temperature, significant reduction of the open circuit voltage was observed, due to excess tunneling which is attributed to the sharpening of band bending. Finally we studied the photovoltaic properties of oxide-oxide junctions and we have observed the change in the open circuit voltage possibly caused by the electron correlation. Through this study, we have revealed the importance of detailed understanding of the electrical properties of the oxide junctions for the improvement of the photocarrier injection technique.

Based on the results, we would like to consider the maximization of the efficiency of the photocarrier injection. In order to store large number of carriers, the depletion layer capacitance should be large. Maximization of V_{OC} is also important. Maximum V_{OC} is limited by the barrier height of the junction. Furthermore, it is important to reduce the recombination processes of injected carriers, which suppress the maximum V_{OC} and reduce the number of stored carriers.

$SrTiO_3$ is one of the most suitable materials for photocarrier injection because of the large permittivity, lattice match to other oxides, and well established surface treatment method [60]. However, because of the temperature and the field dependent permittivity in $SrTiO_3$, efficiency of photocarrier injection can be extremely reduced especially at

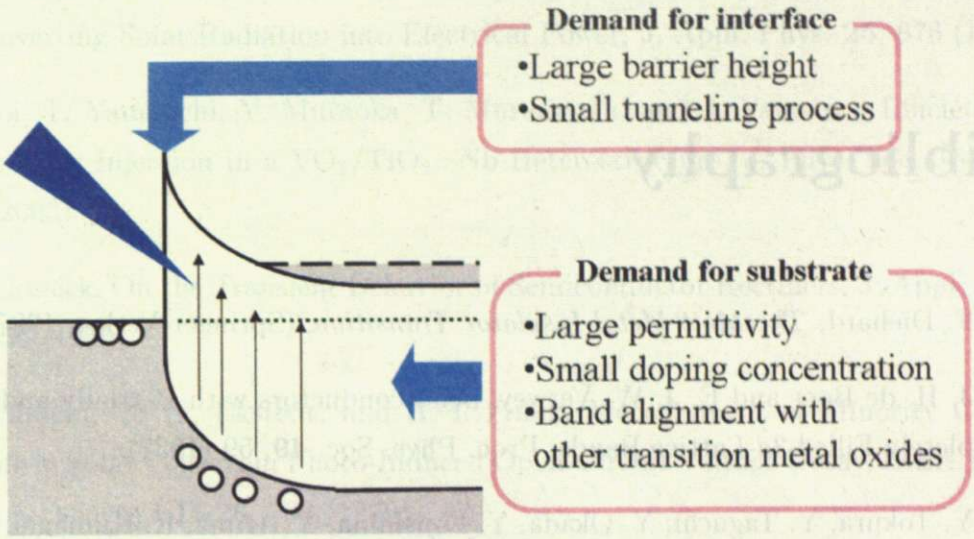

Figure 7.1: A guideline for further improvement of photocarrier injection.

low temperature. Many fascinating phenomena in perovskite oxides are observed at low temperature, so this effect must be removed for the improvement of photocarrier injection. One simple solution is the fabrication of metal-insulator-semiconductor (MIS) structure. An insulating layer reduces the tunneling current induced by band bending. Another possibility is to reduce the internal electric field. For example, using $SrTiO_3$ substrate with lower doping concentration reduces the internal electric field at the interface and suppresses the reduction of the permittivity of $SrTiO_3$. Photo-doping may also be efficient for this purpose. It may also be interesting to find new materials as a substrate. In such case we should consider the band alignment between transition metal oxides in addition to the large permittivity.

Recently physical properties of electrically carrier doped [61, 62] and optically carrier doped [63] $SrTiO_3$ has been studied intensively, and these studies reveal the importance of the electrical and optical carrier doping to the oxides in general. We hope our study can help the understanding of improvement of the photocarrier injection method.

Bibliography

[1] F. Diehard, *The Mott Metal-Insulator Transition*, (Springer-Verlag, 1997).

[2] J. H. de Boer and E. J. W. Verwey, Semi-conductors with Partially and with Completely Filled $3d$-Lattice Bands, Proc. Phys. Soc. **49**, 59 (1937).

[3] Y. Tokura, Y. Taguchi, Y. Okada, Y. Fujishima, T. Arima, K. Kumagai, and Y. Iye, Filling Dependence of Electronic Properties on the Verge of Metal-Mott-Insulator Transition in $Sr_{1-x}La_xTiO_3$, Phys. Rev. Lett. **70**, 2126 (1993).

[4] T. F. Rosenbaum, K. Andres, G. A. Thomas, and R. N. Bhatt, Sharp Metal-Insulator Transition in a Random Solid, Phys. Rev. Lett. **45**, 1723 (1980).

[5] J. Mannhart, High-T_c Transistors, Supercond. Sci. Technol. **9**, 49 (1996).

[6] C. H. Ahn, S. Gariglio, P. Paruch, T. Tybell, L. Antognazza, and J.-M. Triscone, Electrostatic Modulation of Superconductivity in Ultra-Thin $GdBa_2Cu_3O_7$ Films, Science **284**, 1152 (1999).

[7] C. H. Ahn, J.-M. Triscone, and J. Mannhart, Electric Field Effect in Correlated Oxide Systems, Nature **424**, 1015 (2003).

[8] H. Katsu, H. Tanaka, and T. Kawai, Photocarrier Injection Effect on Double Exchange Ferromagnetism in $(La, Sr)MnO_3/SrTiO_3$ Heterostructure, Appl. Phys. Lett. **76**, 3245 (2000).

[9] Y. Muraoka, T. Yamauchi, T. Muramatsu, J. Yamaura, and Z. Hiroi, Efficient Photocarrier Injection to Transition Metal Oxides, J. Mag. Mag. Mater. **272-276**, 448 (2004).

[10] S. M. Sze, *Physics of Semiconductor Devices* 2nd ed. (John Wiley & Sons, Inc., 1981).

[11] S. Kurtin, T.C. McGill, and C. A. Mead, Fundamental Transition in the Electronic Nature of Solids, Phys. Rev. Lett. **22**, 1433 (1969).

[12] F. A. Padovani and R. Stratton, Field and Thermionic-Field Emission in Schottky Barriers, Solid State Electron. **9**, 695 (1966).

[13] D. M. Chapin, C. S. Fuller, and G. L. Pearson, A New Silicon p-n Junction Photocell for Converting Solar Radiation into Electrical Power, J. Appl. Phys. **25**, 676 (1954).

[14] Z. Hiroi, T. Yamauchi, Y. Muraoka, T. Muramatsu, and J. Yamaura, Efficiency of Photocarrier Injection in a $VO_2/TiO_2 : Nb$ Heterostructure, J. Phys. Soc. Jpn. **72**, 3049 (2003).

[15] B. R. Gossick, On the Transient Behavior of Semiconductor Rectifiers, J. Appl. Phys. **26**, 1356 (1955).

[16] J. E. Mahan, T. W. Ekstedt, and R. I. Frank, Measurement of Minority Carrier Lifetime in Solar Cells from Photo-Induced Open-Circuit Voltage Decay, IEEE Trans. Electron Devices **ED-26**, 733 (1979).

[17] P. G. Wilson, Recombination in Silicon p-π-n Diodes, Solid State Electron. **10**, 145 (1967).

[18] R. J. Bassett, Observations on a Method of Determining the Carrier Lifetime in p^+-ν-n^+ Diode, Solid State Electron. **12**, 385 (1969).

[19] J. E. Mahan and D. L. Barnes, Depletion Layer Effects in the Open-Circuit-Voltage-Decay Lifetime Measurement, Solid State Electron. **24**, 989 (1981).

[20] H. Unoki and T. Sakudo, Electron Spin Resonance of Fe^{3+} in $SrTiO_3$ with Special Reference to the 110°K Phase Transition, J. Phys. Soc. Jpn. **23**, 546 (1967).

[21] L. F. Mattheiss, Energy Bands for $KNiF_3$, $SrTiO_3$, $KMoO_3$, and $KTaO_3$, Phys. Rev. B **6**, 4718 (1972).

[22] H. P. R. Frederikse, W. R. Thurber and W. R. Hosler, Electron Transport in Strontium Titanate, Phys. Rev. **134**, A442 (1967).

[23] O. N. Tufte and P. W. Chapman, Electron Mobility in Semiconducting Stontium Titanate, Phys. Rev. **155**, 796 (1967).

[24] C. Lee J. Yahia, and J. L. Brebner, Electron Conduction in Slightly Reduced Strontium Titanate at Low Temperature, Phys. Rev. B **3**, 2525 (1971).

[25] T. Sakudo and H. Unoki, Dielectric Properties of $SrTiO_3$ at Low Temperatures, Phys. Rev. Lett. **26**, 851 (1971).

[26] H. Yasunaga, I. Nakada, Photoconduction of Strontium Titanate, J. Phys. Soc. Jpn. **22**, 338 (1967).

[27] T. Feng, Anomalous Photoelectronic Processes in $SrTiO_3$, Phys. Rev. B **25**, 627 (1982).

[28] H. Katsu, H. Tanaka, and T. Kawai, Anomalous Photoconductivity in $SrTiO_3$, Jpn. J. Appl. Phys. **39**, 2657 (2000).

[29] J. Robertson and C. W. Chen, Schottky Barrier Heights of Tantalum Oxides, Barium Strontium Titanate, Lead Titanate, and Strontium Bismuth Tantalate, Appl. Phys. Lett. **74**, 1168 (1999).

[30] R. V. Neville and C. A. Mead, Surface Barrier Energies of Strontium Titanate, J. Appl. Phys. **43**, 4657 (1972).

[31] F. J. Morin and T. Wolfram, Surface States and Catalysis on *d*-Band Perovskites, Phys. Rev. Lett. **30**, 1214 (1973).

[32] R. A. Powell and W. E. Spicer, Photoemission Investigation of Surface States on Strontium Titanate, Phys. Rev. B **13**, 2601 (1976).

[33] H. Hasegawa and T. Nishio, Electrical Properties of Au/Nb-doped $SrTiO_3$ Contact, J. Appl. Phys. **69**, 1501 (1991).

[34] T. Shimizu and H. Okushi, Intrinsic Electrical Properties of Au/$SrTiO_3$ Schottky Junctions, J. Appl. Phys. **85**, 7244 (1999).

[35] J. H. Barrett, Dielectric Constant in Perovskite Type Crystals, Phys. Rev. **86**, 118 (1951).

[36] S. Suzuki, T. Yamamoto, H. Suzuki, K. Kawaguchi, K. Takahashi, and Y. Yoshisato, Fabrication and Characterization of $Ba_{1-x}K_xBiO_3$/Nb-doped $SrTiO_3$ All-Oxide-Type Schottky Junctions, J. Appl. Phys. **81**, 6830 (1997).

[37] T. Yamamoto, S. Suzuki, K. Kawaguchi, and K. Takahashi, Temperature Dependence of the Ideality Factor of of $Ba_{1-x}K_xBiO_3$/Nb-doped $SrTiO_3$ All-Oxide-Type Schottky Junctions, Jpn. J. Appl. Phys. **37**, 4737 (1998).

[38] H.-M Christen, J. Mannhart, E. J. Williams, and Ch. Gerber, Dielectric Properties of Sputtered $SrTiO_3$ films, Phys. Rev. B **49**, 12095 (1994).

[39] T. Susaki, Y. Kozuka, Y. Tateyama, and H. Y. Hwang, Temperature-Dependent Polarity Reversal in of Au/Nb : $SrTiO_3$ Schottky Junctions, Phys. Rev. B **76**, 155110 (2007).

[40] M. I. Cohen and R. F. Brunt, Optical Properties of $SrTiO_3$ in the Region of the Absorption Edge, Phys. Rev. **168**, 929 (1968).

[41] M. Capizzi and A. Frova, Optical Gap of Strontium Titanate (Deviation from Urbach Tail Behavior), Phys. Rev. Lett. **25**, 1298 (1970).

[42] K. C. Kao, *Dielectric Phenomena in Solids*, (Elsevier Academic Press, 2004).

[43] C. Ito, M. Sasabe, and H. Kida, Drift Mobility of Charge Carriers in Crystalline $SrTiO_3$ Measured by Time-of-Flight Photoconductivity, JPS Spring Meeting 28p XK-5 (2004).

[44] A. Lagendijk, M. Glasbeek, and J.D.W. Van Voorst, Paramagnetic Oxygen Centers in $SrTiO_3$ Induced by Light, Chem. Phys. Lett. **20**, 92 (1973).

[45] Y. Hikita, Ph. D Thesis, University of Tokyo (2007).

[46] Z. Sroubek, Electron Tunneling and Band Structure of $SrTiO_3$ and $KaTaO_3$, Phys. Rev. B **2**, 3170 (1970).

[47] T. Hasegawa, M. Shirai and K. Tanaka, Localizing Nature of Photo Excited States in $SrTiO_3$, J. Luminescence **87-89**, 1217 (2000).

[48] M. K. Sheinkman and A. Ya. Shik, Long-Term Relaxation and Residual Conductivity of Semiconductor (Review), Sov. Phys. Semicond. **10**, 128 (2000).

[49] T. Fujii, M. Kawasaki, A. Sawa and H. Akoh, Y. Kawazoe, and Y. Tokura, Histeric Current-Voltage Characteristics and Resistance Switching at an Epitaxial Oxide Schottky Junction $SrRuO_3/SrTi_{0.99}Nb_{0.01}O_3$, Appl. Phys. Lett. **86**, 012107 (2005).

[50] N. Nakagawa, M. Asai, Y. Mukunoki, T. Susaki, and H. Y. Hwang, Magnetocapacitance and Exponential Magnetoresistance in Manganite-Titanate Heterojunctions, Appl. Phys. Lett. **86**, 082504 (2005).

[51] A. Urushibara, Y. Morimoto, T. Arima and Y. Tokura, Insulator Metal Transition and Giant Magnetoresistance in $La_{1-x}Sr_xMnO_3$, Phys. Rev. B **51**, 14103 (1995).

[52] Y. Tokura, Critical Features of Colossal Magnetoresistive Manganites, Rep. Prog. Phys. **69**, 797 (2006).

[53] H. Y. Hwang, S-W. Cheong, P. G. Rasaelli, M. Marezio, and B. Batlogg, Lattice Effects on the Magnetorisistance in Doped $LaMnO_3$, Phys. Rev. Lett. **75**, 914 (1995).

[54] Y. Okimoto, T. Katsufuji, T. Ishikawa, T. Arima, and Y. Tokura, Variation of Electronic Structure in $La_{1-x}Sr_xMnO_3$ ($0 \leq x \leq 0.3$) as Investigated by Optical Conductivity Spectra, Phys. Rev. B **55**, 4206 (1997).

[55] T. Saitoh, A. E. Bocquet, T. Mizokawa, H. Namatame, A. Fujimori, M. Abbate, Y. Takeda, and M. Takano, Electronic Structure of $La_{1-x}Sr_xMnO_3$ Studied by Photoemission and X-Ray-Absorption Spectroscopy, Phys. Rev. B **51**, 13942 (1995).

[56] A. Sawa, A. Yamamoto, H. Yamada, T. Fujii, M. Kawasaki, J. Matsuno, and Y. Tokura, Fermi Level Shift in $La_{1-x}Sr_xMO_3$ (M = Mn, Fe, Co, and Ni) Probed by Schottky-Like Heteroepitaxial Junctions with $SrTi_{0.99}Nb_{001}O_3$, Appl. Phys. Lett. **90**, 252102 (2007).

[57] J. Matsuno, A. Fujimori, Y. Takeda, and M. Takano, Chemical potential shift in $La_{1-x}Sr_xMnO_3$: Photoemission Test of the Phase Separation Senario, Europhys. Lett. **59**, 252 (2002).

[58] D. W. Reagor, S. Y. Lee, Y. Li, and Q. X. Jia, Work Function of the Mixed-Valent Manganese Perovskites, J. Appl. Phys. **95**, 7971 (2004).

[59] R. L. Anderson, Experiments on Ge-GaAs Heterojunctions, Solid State Electron. **5**, 341 (1962).

[60] M. Kawasaki, K. Takahashi, T. Maeda, R. Tsuchiya, M. Shinohara, O. Ishiyama, T. Yonezawa, M. Yoshimoto, and H. Koinuma, Atomic Control of the $SrTiO_3$ Crystal Surface, Science **266**, 1540 (1994).

[61] A. Ohtomo and H. Y. Hwang, A High-Mobility Electron Gas at the $LaAlO_3/SrTiO_3$ Heterointerface, Nature **427**, 423 (2004).

[62] H. Nakamura, H. Takagi, I. H. Inoue, Y. Takahashi, T. Hasegawa, and Y. Tokura, Low Temperature Metallic State Induced by Electrostatic Carrier Doping of $SrTiO_3$, Appl. Phys. Lett. **89**, 133504 (2006).

[63] Y. Kozuka, Y. Hikita, T. Susaki, and H. Y. Hwang, Optically Tuned Dimensionality Crossover in Photocarrier-Doped $SrTiO_3$: Onset of Weak Localization, Phys. Rev. B **76**, 085129 (2007).

Acknowledgments

First of all, I would like to express my sincere gratitude to Prof. Harold Y. Hwang for his supervision on the present thesis. When I was struggling how to procede my study, he always gave me suggestive and helpful ideas. This work would not have been possible without his kind advice and encouragement. I have been inspired very much by his attitude toward science and I have learned how to enjoy interesting science from him.

I would also like to express my deep gratitude to assistant professor Dr. Yasuyuki Hikita for continuous guidance. He also taught me how to use the optical measurment system (Photon-man) in which most of the experiments were carried out. Prof. Tomofumi Susaki, a former research associate of Hwang lab. in Tokyo Institute of Technology also helped me in both in science and in maintaining good lab environment. I am grateful for his kind instruction to my study. Mr.Yusuke Kozuka supported me from closest position and gave me many advices. His advices helps me to proceed this work.

I would also like to appreciate Prof. Mikk Lippmaa and Dr. Tsuyoshi Onishi at the Institue for Solid State Physics. University of Tokyo for technical support and helpful comments on my study.

Former laboratory post-doc, Prof. Jong Hyun Song in Chungnam National University, provided me manganite samples and I would like to appreciate his cooperation. I would like to thank Dr. Christpher Bell for advice for my research and instruction about many equipments. Dr. Yi Zhao also gave me useful comments about my study. I also feel grateful for the former laboratory members Dr. Yasushi Hotta, Dr. Shunsuke Tsuda abd Dr. Kei Takahashi. Especially Dr. Tsuda supported my first year of master cource and his knowledge about photoemission and optical spectroscopy was very helpful. I would also like to thank laboratory members, Mr. Takuya Higuchi, Mr. Takeaki Yajima, Mr. Yusuke Ota, Mr. Mitsuru Nishikawa, and Mr. Masayuki Hosoda and former laboratory members Mr. Yasushige Mukunoki, Mr. Luuk van Rees, and Mr. Shin Yoshida for daily disscussion. Finally I would like to thank Ms. Makiko Tanaka, the seculetary for her daily support.